University of Groningen

Lyα Forest Tomography from Background Galaxies: The First Megaparsec-resolution Large-scale Structure Map at z > 2

Lee, Khee-Gan; Hennawi, Joseph F.; Stark, Casey; Prochaska, J. Xavier; White, Martin; Schlegel, David J.; Eilers, Anna-Christina; Arinyo-i-Prats, Andreu; Suzuki, Nao; Croft, Rupert A. C.

IMPORTANT NOTE: You are advised to consult the publisher's version (publisher's PDF) if you wish to cite from it. Please check the document version below.

Document Version
Publisher's PDF, also known as Version of record

Link to publication in University of Groningen/UMCG research database

LYα FOREST TOMOGRAPHY FROM BACKGROUND GALAXIES: THE FIRST MEGAPARSEC-RESOLUTION LARGE-SCALE STRUCTURE MAP AT $z > 2$

Khee-Gan Lee[1], Joseph F. Hennawi[1], Casey Stark[2,3], J. Xavier Prochaska[4,5], Martin White[2,3],
David J. Schlegel[5], Anna-Christina Eilers[1], Andreu Arinyo-i-Prats[6], Nao Suzuki[7], Rupert A. C. Croft[8],
Karina I. Caputi[9], Paolo Cassata[10,11], Olivier Ilbert[11], Bianca Garilli[12], Anton M. Koekemoer[13],
Vincent Le Brun[11], Olivier Le Fèvre[11], Dario Maccagni[14], Peter Nugent[3,2], Yoshiaki Taniguchi[15],
Lidia A. M. Tasca[11], Laurence Tresse[11], Gianni Zamorani[14], and Elena Zucca[14]

[1] Max Planck Institute for Astronomy, Königstuhl 17, D-69117 Heidelberg, Germany; lee@mpia.de
[2] Department of Astronomy, University of California at Berkeley, B-20 Hearst Field Annex 3411, Berkeley, CA 94720, USA
[3] Lawrence Berkeley National Laboratory, 1 Cyclotron Road, Berkeley, CA 94720, USA
[4] Department of Astronomy and Astrophysics, University of California, 1156 High Street, Santa Cruz, CA 95064, USA
[5] University of California Observatories, Lick Observatory, 1156 High Street, Santa Cruz, CA 95064, USA
[6] Institut de Ciències del Cosmos, Universitat de Barcelona (IEEC-UB), Martí Franquès 1, E-08028 Barcelona, Spain
[7] Kavli Institute for the Physics and Mathematics of the Universe (IPMU), The University of Tokyo, Kashiwano-ha 5-1-5, Kashiwa-shi, Chiba, Japan
[8] Department of Physics, Carnegie Mellon University, 5000 Forbes Avenue, Pittsburgh, PA 15213, USA
[9] Kapteyn Astronomical Institute, University of Groningen, P.O. Box 800, 9700-AV Groningen, The Netherlands
[10] Instituto de Fisica y Astronomia, Facultad de Ciencias, Universidad de Valparaiso, Av. Gran Bretana 1111, Casilla 5030, Valparaiso, Chile
[11] Aix Marseille Université, CNRS, LAM (Laboratoire d'Astrophysique de Marseille) UMR 7326, F-13388 Marseille, France
[12] INAF–IASF, Via Bassini 15, I-20133, Milano, Italy
[13] Space Telescope Science Institute, 3700 San Martin Drive, Baltimore, MD 21218, USA
[14] INAF–Osservatorio Astronomico di Bologna, Via Ranzani,1, I-40127 Bologna, Italy
[15] Research Center for Space and Cosmic Evolution, Ehime University, 2-5 Bunkyo-cho, Matsuyama 790-8577, Japan

ABSTRACT

We present the first observations of foreground Lyα forest absorption from high-redshift galaxies, targeting 24 star-forming galaxies (SFGs) with $z \sim 2.3$–2.8 within a $5' \times 14'$ region of the COSMOS field. The transverse sightline separation is $\sim 2\,h^{-1}$ Mpc comoving, allowing us to create a tomographic reconstruction of the three-dimensional (3D) Lyα forest absorption field over the redshift range $2.20 \leqslant z \leqslant 2.45$. The resulting map covers $6\,h^{-1}$ Mpc $\times 14\,h^{-1}$ Mpc in the transverse plane and $230\,h^{-1}$ Mpc along the line of sight with a spatial resolution of $\approx 3.5\,h^{-1}$ Mpc, and is the first high-fidelity map of a large-scale structure on $\sim$ Mpc scales at $z > 2$. Our map reveals significant structures with $\gtrsim 10\,h^{-1}$ Mpc extent, including several spanning the entire transverse breadth, providing qualitative evidence for the filamentary structures predicted to exist in the high-redshift cosmic web. Simulated reconstructions with the same sightline sampling, spectral resolution, and signal-to-noise ratio recover the salient structures present in the underlying 3D absorption fields. Using data from other surveys, we identified 18 galaxies with known redshifts coeval with our map volume, enabling a direct comparison with our tomographic map. This shows that galaxies preferentially occupy high-density regions, in qualitative agreement with the same comparison applied to simulations. Our results establish the feasibility of the CLAMATO survey, which aims to obtain Lyα forest spectra for ~ 1000 SFGs over ~ 1 deg^2 of the COSMOS field, in order to map out the intergalactic medium large-scale structure at $\langle z \rangle \sim 2.3$ over a large volume $(100\,h^{-1}$ Mpc$)^3$.

Key words: cosmology: observations – galaxies: high-redshift – intergalactic medium – quasars: absorption lines – surveys – techniques: spectroscopic

Online-only material: color figures

1. INTRODUCTION

The Lyα "forest" absorption seen in quasar spectra is a crucial probe of the intergalactic medium (IGM). In the modern "fluctuating Gunn–Peterson" scenario (Cen et al. 1994; Bi et al. 1995; Croft et al. 1998; Hui et al. 1997), this is from residual neutral hydrogen in photoionization equilibrium, tracing the underlying density field, allowing the study of a large-scale structure (LSS) at $z \gtrsim 2$ (e.g., Croft et al. 2002; McDonald et al. 2006; Busca et al. 2013; Palanque-Delabrouille et al. 2013; Delubac et al. 2014).

The Lyα forest observed in individual quasars probe the IGM along one dimension (1D), but, using multiple spectra with small transverse separations, it is possible to "tomographically" reconstruct a three-dimensional (3D) map of the Lyα forest absorption (Pichon et al. 2001; Caucci et al. 2008; Cisewski

et al. 2014; Lee et al. 2014a, hereafter L14). The effective spatial resolution, ϵ_{3D}, of such a map is determined by the transverse sightline separation, $\langle d_\perp \rangle$. This probes $\sim$ Mpc scales only by exploiting UV-bright star-forming galaxies (SFGs) as background sources in addition to quasars. However, SFGs are faint ($g \gtrsim 23$)—even with 8–10 m telescopes, only spectral signal-to-noise ratios (S/Ns) of a few are feasible from such objects, assuming reasonable exposure times. However, L14 argued that such data at moderate resolutions ($R \equiv \lambda/\Delta(\lambda) \sim 1000$) are adequate for Lyα forest tomography that resolve the LSS on scales of $\epsilon_{3D} \sim 2$–$5\,h^{-1}$ Mpc.

In this Letter, we describe pilot observations for the COS-MOS Lyman-Alpha Mapping And Tomography Observations (CLAMATO) survey. The full survey is aimed at mapping the $z \sim 2.3$ IGM within ~ 1 deg^2 of the COSMOS field (Scoville et al. 2007). The pilot observations were, however, limited to

one half-night of successful data, yielding moderate-resolution spectra for 24 SFGs at $g \leqslant 24.9$ within $\sim 5' \times 14'$.

This data represents, to our knowledge, the first systematic attempt to exploit spectra of unlensed high-redshift SFGs for Lyα forest analysis. Our background sources are ~ 2.5–3 mag fainter than existing Lyα forest data sets (e.g., $g \sim 21.5$ in BOSS; Dawson et al. 2013), yielding ~ 100 greater area density of sightlines ($\sim 1000 \deg^{-2}$ versus $\sim 15 \deg^{-2}$ in BOSS). This dramatic increase results in small average inter-sightline separations ($\langle d_\perp \rangle \sim 2.3 \, h^{-1}$ Mpc), enabling a tomographic reconstruction of the 3D Lyα forest absorption, providing an unprecedented view of the $z > 2$ cosmic web on scales of several comoving megaparsecs. As we shall see, comparisons with a small number of coeval galaxies as well as simulated reconstructions indicate that the map is indeed tracing LSS.

In this Letter, we assume a concordance flat ΛCDM cosmology with $\Omega_M = 0.26$, $\Omega_\Lambda = 0.74$, and $H_0 = 70 \, \mathrm{km \, s^{-1}}$.

2. OBSERVATIONS AND DATA REDUCTION

Our observations target g-selected galaxies and active galactic nuclei (using the Capak et al. 2007 photometry) at $2.3 < z_{\mathrm{bg}} < 3$, such that their Ly$\alpha$ forest absorption covers $2.15 \leqslant z_\alpha \leqslant 2.40$. By working in the COSMOS field (Scoville et al. 2007), we are able to exploit rich multiwavelength imaging and spectroscopy to efficiently target the necessary background sources. Our primary candidates are spectroscopically confirmed objects from the zCOSMOS-Deep (Lilly et al. 2007) and VUDS (Le Fevre et al. 2014) surveys—we reobserve these to obtain adequate S/N and spectral resolution for tomography. Where available, we also added grism redshifts kindly provided by the 3D-HST team (e.g., Brammer et al. 2012). Beyond spectroscopically confirmed candidates, we add photometric redshifts from Ilbert et al. (2009) as well as Salvato et al. (2011) for X-ray-detected sources. From these candidates, we selected targets based on redshift probability, source brightness, and uniformity on the sky—the selection functions of the source catalogs are unimportant to us since the background source properties do not bias the foreground absorption.

We observed with the Low Resolution Imaging Spectrometer (LRIS) Double-Spectrograph (Oke et al. 1995; Steidel et al. 2004) on the Keck-I Telescope at Mauna Kea, HI, from 2014 March 26–27 and 29–30, in MOS mode with the B600/4000 grism on the blue arm and R600/5000 grating on the red with the d500 dichroic. With 1″ slits, this yields $R \equiv \lambda/\Delta\lambda \approx 1000$ and $R \approx 1200$ for the blue and red arms, respectively. We suffered a $\sim 70\%$ weather loss, but obtained good quality spectra for two slitmasks covering $\sim 5' \times 14'$, with total exposure times of 6600–7200 s in 0″.5–0″.7 seeing and clear conditions. These two slitmasks overlap along their short edge, resulting in an elongated footprint (Figure 1).

The data were reduced with the XIDL package,[16] and visually inspected to determine source redshifts. Out of 47 targeted objects, we successfully extracted 1D spectra and estimated redshifts for 33, of which 24 were determined to have the correct redshift and adequate spectral S/N to contribute to our tomographic reconstruction. The number of sources within our nominal $g \leqslant 24.5$ survey limit is $\sim 50\%$ of that estimated by L14, a shortfall that was already evident during the target-selection process. This is likely because L14 did not take into account dust-reddening ($E(B - V) \sim 0.2$; Reddy et al. 2008) when estimating source counts—the SFG luminosity
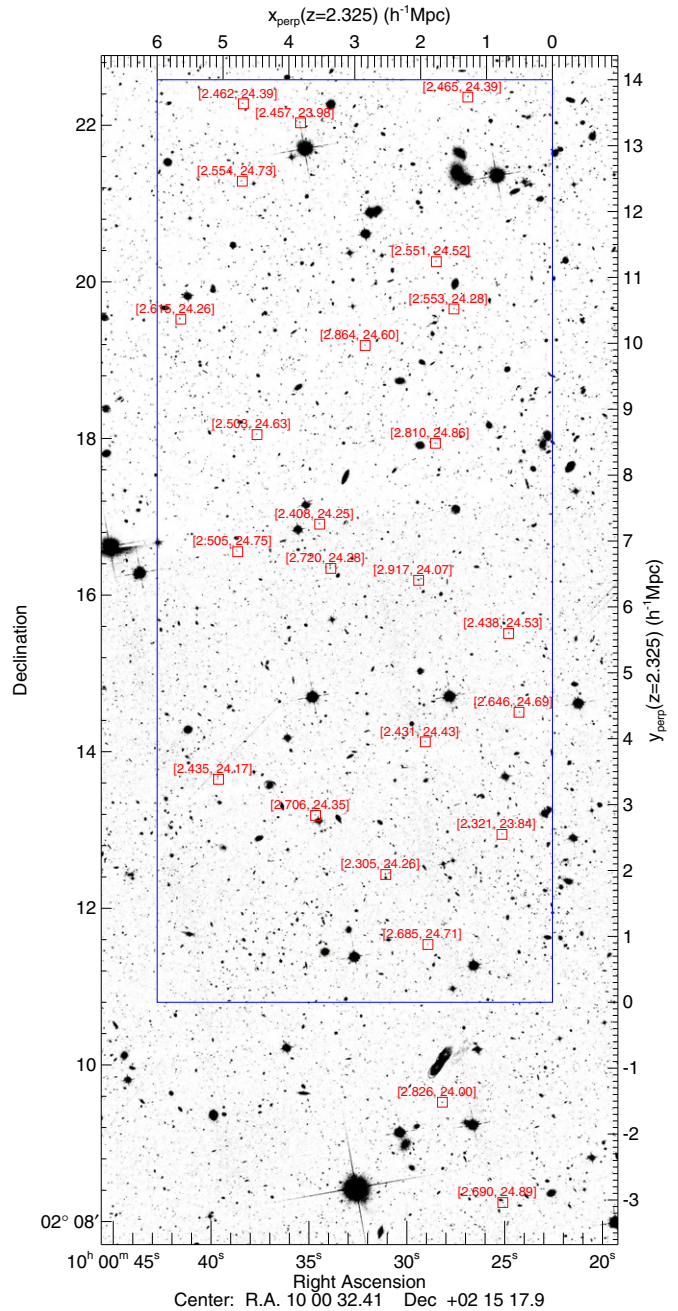

Figure 1. *Hubble Space Telescope* Advanced Camera for Surveys F814W mosaic (Koekemoer et al. 2007) of our target region. The red boxes indicate our background spectroscopic sources with Lyα forest coverage over $2.15 \leqslant z_\alpha \leqslant 2.40$; source redshifts and g magnitudes are labeled above each object. The transverse area of our map is bounded in blue; the top and right axes indicate the transverse comoving separation at $z = 2.325$ relative to the map coordinate origins.

(A color version of this figure is available in the online journal.)

---

function is so steep that even small errors in the assumed magnitudes could easily lead to this $\sim 50\%$ discrepancy. To fill the slitmasks, we therefore also targeted $g > 24.5$ objects, but these were less likely to be successfully reduced or have adequate S/N. Nevertheless, even this reduced number of sources is sufficient to carry out Lyα forest tomography, as we shall see.

The position of the 24 SFGs on the sky are shown in Figure 1. Our brightest objects are $g \approx 24.0$ SFGs with S/N ≈ 3–4
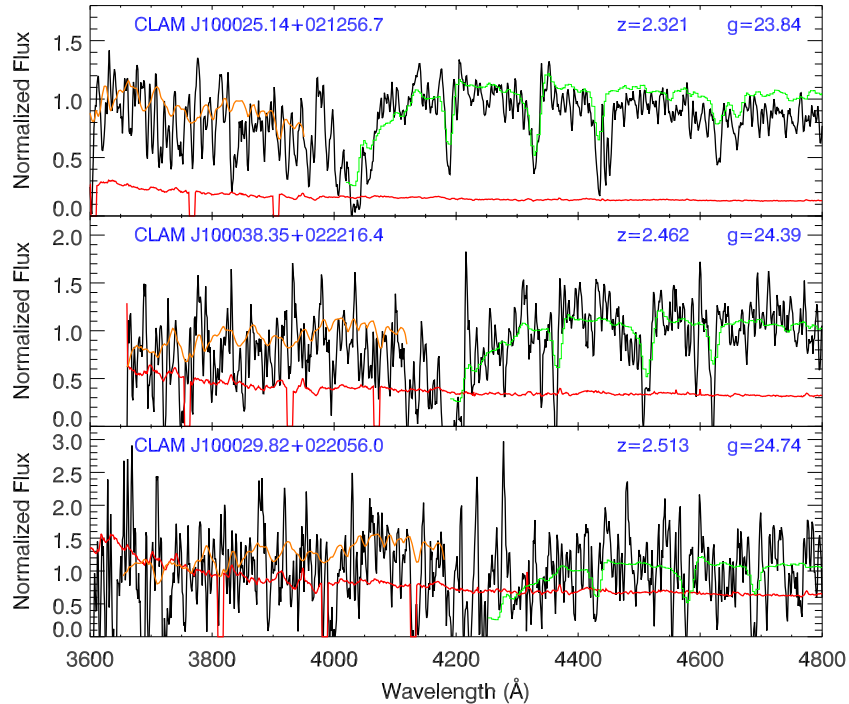

Figure 2. Examples of SFG spectra obtained with Keck LRIS and subsequently used for Lyα forest tomographic reconstruction. From top to bottom, these represent our highest, median, and lowest S/N spectra, respectively. The red curve represents the estimated pixel noise, with masked pixels (mostly intrinsic absorption lines) set to zero. The green curve is the Shapley et al. (2003) composite Lyman-break galaxy spectrum overplotted at the source redshifts, while the orange curve is the estimated continuum (see the text).

(A color version of this figure is available in the online journal.)

per 1.2 Å pixel, while on the faint end we use spectra down to S/N ≈ 1.3 from $g \approx 24.8$ sources. Examples of the spectra are shown in Figure 2. We also attempted to visually identify damped Lyα absorbers that might affect Lyα forest analysis but found none.

To extract the Lyα forest transmission from the spectra, we need to estimate the intrinsic "continuum" of the SFGs. Studies of $z \sim 3$ SFG composite spectra (Shapley et al. 2003; Berry et al. 2012) suggest that this is relatively flat in the Lyα forest region, with only a few strong intrinsic absorbers visible—this is corroborated by high-resolution line analysis of the lensed galaxy MS1512-cB58 (Savaglio et al. 2002). From these studies, we determined that the strongest intrinsic absorption within the 1040–1190 Å Lyα forest region are at N II λ1084.0, N I λ1134.4, and C III λ1175.7—we mask ±5 Å around these transitions. We then adopt as our continuum template the restframe composite spectrum of 59 SFGs from Berry et al. (2012), in which the Lyα forest variance in the restframe ∼1040–1190 Å region have been smoothed out through averaging, albeit with an overall absorption decrement.

Using this template, we estimate the continuum, C, for each individual spectrum by "mean-flux regulation" (Lee et al. 2012, 2013), i.e., adjusting the amplitude and slope of the 1040–1190 Å continuum template until the mean Lyα forest transmission, $\langle F \rangle(z)$, from each spectrum agrees with the measurements of Becker et al. (2013). This method ensures that there is no overall bias in the resulting continua. We estimate the continuum error to be ≲10%, by considering the variation of Starburst99 (Leitherer et al. 1999, 2010) models with respect to various physical parameters. This is adequate for our S/N ⩽ 4 spectra, but in future papers we will study SFG continuum-fitting in more detail.

We divide the restframe 1040–1190 Å flux, f, from each spectrum by the continuum to obtain the Lyα forest transmission $F = f/C$, and further the forest fluctuations:

$$\delta_F = F/\langle F \rangle(z) - 1. \tag{1}$$

We also compute the error, $\sigma_N = \sigma/C/\langle F \rangle(z)$, where σ is the pixel noise reported by the reduction pipeline. The vectors of δ_F and σ_N, along with the corresponding 3D pixel positions, constitute the inputs for the tomographic reconstruction.

3. TOMOGRAPHIC RECONSTRUCTION

To create the Lyα forest tomographic reconstruction, we use Wiener filtering (e.g., Wiener 1942; Press et al. 1992; Zaroubi et al. 1995), where the reconstructed field, $\delta_F^{\rm rec}$, is

$$\delta_F^{\rm rec} = \mathbf{C}_{\rm MD} \cdot (\mathbf{C}_{\rm DD} + \mathbf{N})^{-1} \cdot \delta_F, \tag{2}$$

where $\mathbf{C}_{\rm DD} + \mathbf{N}$ and $\mathbf{C}_{\rm MD}$ are the data–data and map–data covariances, respectively. The noise covariance matrix $\mathbf{N}$ is assumed to have only diagonal elements set by the noise variances, $N_{ii} = \sigma_{N,i}^2$. This term allows us to weight each input pixel by its S/N, so lower S/N spectra are down-weighted and avoid noise spikes from biasing the map.

Following L14 and Caucci et al. (2008), we assume that between any two points $\mathbf{r_1}$ and $\mathbf{r_2}$, whether in the maps or skewers, $\mathbf{C}_{\rm DD} = \mathbf{C}_{\rm MD} = \mathbf{C}(\mathbf{r_1}, \mathbf{r_2})$ and

$$\mathbf{C}(\mathbf{r_1}, \mathbf{r_2}) = \sigma_F^2 \exp\left[-\frac{(\Delta r_\parallel)^2}{2L_\parallel^2}\right] \exp\left[-\frac{(\Delta r_\perp)^2}{2L_\perp^2}\right], \tag{3}$$

where $\Delta r_\parallel$ and $\Delta r_\perp$ are the distance between $\mathbf{r_1}$ and $\mathbf{r_2}$ along, and transverse to the line of sight, respectively. $L_\parallel$ and $L_\perp$ are free
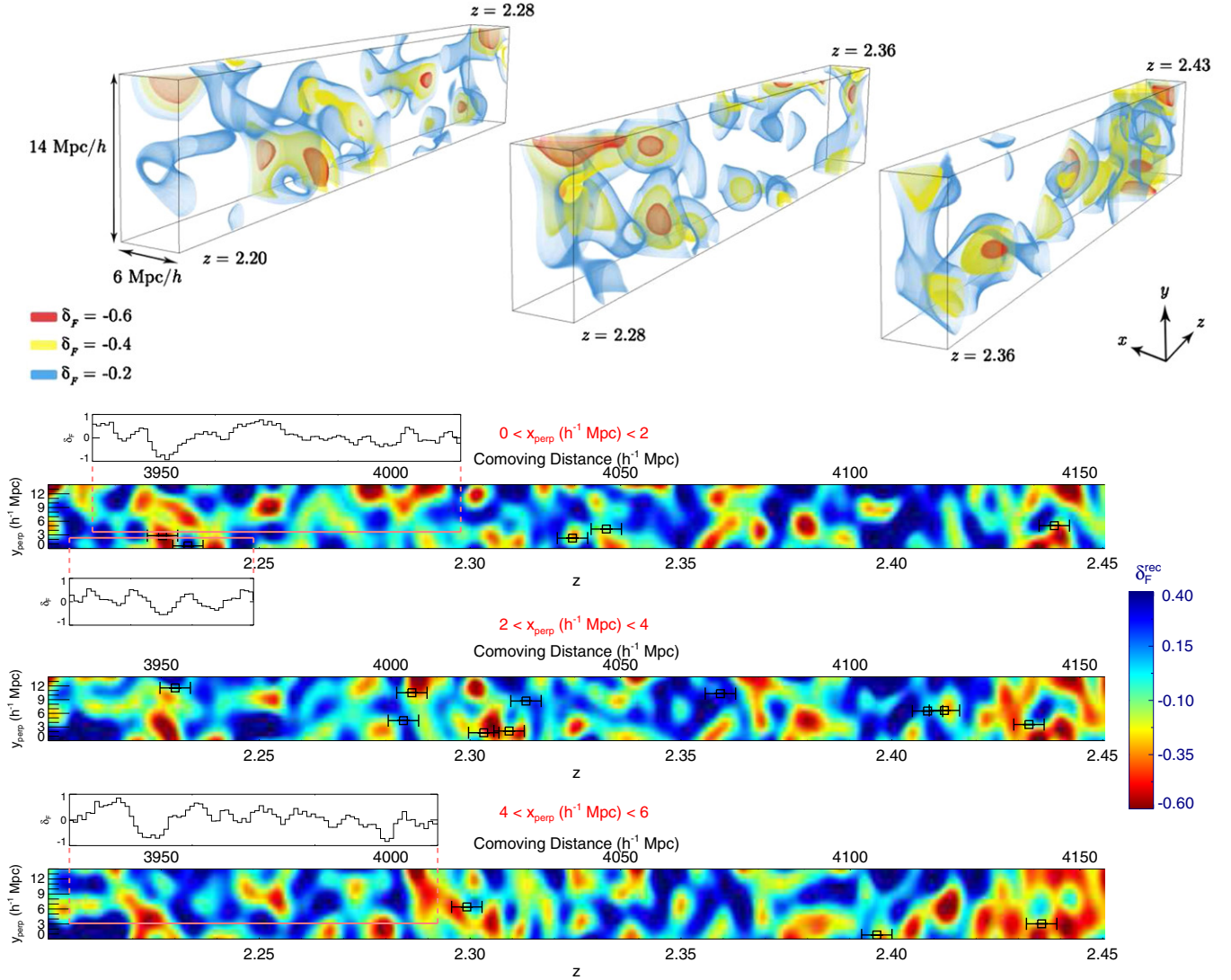
Figure 3. Tomographic reconstruction of 3D Lyα forest absorption from our data, shown in three redshift segments in 3D (top) and projected over three slices along the R.A. direction (bottom panels). The color scale represents reconstructed Lyα forest transmission such that negative values (red) correspond to overdensities. Square symbols denote positions of coeval galaxies within the map; error bars indicate the $\sigma_v \approx 300 \, \mathrm{km \, s^{-1}}$ uncertainty on their redshifts. Pink solid lines indicate where three of the skewers probe the volume, with inset panels indicating the corresponding 1D absorption spectra (top-hat-smoothed by 3 pixels) that contributed to the tomographic reconstruction.

(A color version of this figure is available in the online journal.)

parameters that set the effective smoothing of the reconstruction parallel and perpendicular to the line of sight, respectively, while $\sigma_F = 0.8$ sets the overall correlation strength. These parameters need to be matched to the data quality: we set $L_\parallel = 2.7 \, h^{-1}$ Mpc, roughly the comoving scale along the line of sight corresponding to our spectral resolution element. For $L_\perp$, Caucci et al. (2008) suggested setting it to the typical transverse sightline separation $\langle d_\perp \rangle$, but we choose $L_\perp = 3.5 \, h^{-1}$ Mpc even though our sightline separation is $\langle d_\perp \rangle \approx 2.3 \, h^{-1}$ Mpc. This is a conservative choice taking into account the low S/N of our individual spectra. The choice of these reconstruction parameters is somewhat arbitrary since small changes do not qualitatively change the resulting map features, but in future work we will discuss optimal choices for these parameters.

Our map originates at $[\alpha_0, \delta_0] = [10^h 00' 22^s.56, +02°10'48''.0]$, spanning $[6 \, h^{-1} \, \mathrm{Mpc}, 14 \, h^{-1} \, \mathrm{Mpc}]$ in the $[x_\mathrm{perp}, y_\mathrm{perp}]$ directions on the sky (see the top and right axes in Figure 1); along the line of sight, the origin is $z_\alpha = 2.20$ and

extends $\Delta\chi = 230 \, h^{-1}$ Mpc up to $z_\alpha \approx 2.45$, giving an overall comoving volume of $6 \, h^{-1} \, \mathrm{Mpc} \times 14 \, h^{-1} \, \mathrm{Mpc} \times 230 \, h^{-1} \, \mathrm{Mpc} = 19320 \, h^{-3} \, \mathrm{Mpc^3} \approx (27 \, h^{-1} \, \mathrm{Mpc})^3$. Note that our map does not cover the region $\delta \lesssim 2°11'$, where we experienced a high failure rate in spectral extraction and redshift identification due to deteriorating observing conditions. However, the two spectra in the excluded region are still included in the map input; given our transverse correlation length of $L_\perp = 3.5 \, h^{-1}$ Mpc, these spectra ($\approx 1.5 \, h^{-1}$ Mpc and $\approx 3 \, h^{-1}$ Mpc from the lower map boundary) still contribute to the low-y_perp portions of the map.

We evaluated Equation (2) to solve for the output tomographic map, δ_F^rec, using a preconditioned conjugate-gradient algorithm to carry out the matrix inversion and matrix-vector multiplication (C. Stark et al., in preparation), sampling from a 3D comoving grid with $(0.5 \, h^{-1} \, \mathrm{Mpc})^3$ cells. For simplicity, we assumed a fixed differential comoving distance $d\chi/dz$ (evaluated at $z = 2.325$, the mean map redshift) when setting up the output grid. This avoids a flared map geometry, since the
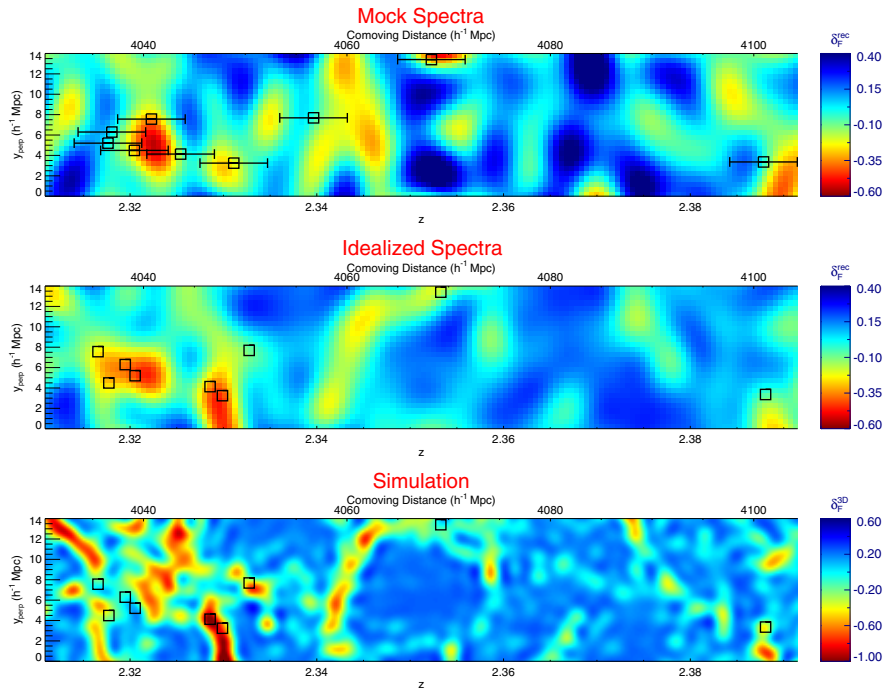
Figure 4. Top: slice from a tomographic reconstruction (projected over $\Delta x_{\rm perp} = 2\,h^{-1}$ Mpc) using a mock data set with similar spatial sampling and S/N to our data. Middle: a reconstruction (with the same $[L_\parallel, L_\perp, \sigma_F]$) from the full grid of noiseless spectra with $0.8\,h^{-1}$ Mpc transverse separations. For reference, the bottom panel shows the "true" absorption field in the simulation. Black squares indicate locations of coeval $R \leqslant 25.5$ galaxies—in the top panel we also introduced random redshift errors.

(A color version of this figure is available in the online journal.)

transverse comoving area increases with redshift, but with our limited redshift range, this effect is small.

The resulting map of the 3D Lyα forest absorption, $\delta_F^{\rm rec}$, is shown in Figure 3 as 3D visualizations and slices projected over the $x_{\rm perp}$ (R.A.) direction. A significant amount of structure is obvious even within this small volume, with overdensities (negative $\delta_F^{\rm rec}$ regions) spanning comoving distances of $\Delta y_{\rm perp} \gtrsim 10\,h^{-1}$ Mpc both along the line of sight (e.g., from $z \approx 2.21$ to $z \approx 2.23$ at $y_{\rm perp} \sim 8\,h^{-1}$ Mpc) and across the transverse direction (at $z \approx 2.43$). The strong overdensities are typically sampled by multiple sightlines at different background redshifts. This is illustrated by inset panels in the map slices in Figure 3, where we show three examples of the 1D absorption field, δ_F, that went into the reconstruction—the overdensity at a comoving distance of $\approx 3950\,h^{-1}$ Mpc and $y_{\rm perp} \leqslant 5\,h^{-1}$ Mpc can be seen as clear dips in all three of the spectra, which is unlikely to be caused by pixel noise. Note that in moderate-resolution Lyα forest data, significant "absorbers" are typically due to blends of clustered Lyα forest absorption and not individual absorbers (Lee et al. 2014b; Pieri et al. 2014). One also clearly sees significant voids (dark blue regions) on scales of ~ 5–$10\,h^{-1}$ Mpc.

As validation, we performed reconstructions on mock data sets derived from simulations (e.g., L14). These mocks have identical sightline configurations, resolution, and S/N as the data, including random continuum errors with 7% rms. The resulting reconstructions are illustrated in Figure 4, compared with the "true" absorption field from the simulation. The good correspondence between large-scale features in the "true" and reconstructed fields gives us confidence that the real map (Figure 3) is indeed probing LSS. However, the probability distribution function (PDF) of the simulated reconstructions differed from

the real map (see the black histograms in Figures 5(a) and (b)). To investigate, we ran 24 mock reconstructions on independent simulation volumes, which showed considerable scatter in the resulting PDFs (gray shaded area in Figure 5(b)). This suggests that part of the discrepancy is due to cosmic variance from our small volume. Moreover, while dark matter-only simulations correctly reproduce Lyα forest clustering, they do not yield the right PDF (White et al. 2010), which could also contribute to the disagreement.

4. COMPARISON WITH COEVAL GALAXIES

Since galaxies are well-known tracers of LSSs, we can exploit the spectroscopically confirmed high-redshift galaxies within the COSMOS field (Lilly et al. 2007; Le Fevre et al. 2014) to make a comparison with our Lyα forest tomographic map. We searched an internal COSMOS compilation of all available spectroscopic redshifts, and found 18 galaxies coeval within the map volume (4 were uniquely confirmed by our observations). This small number is clearly inadequate for mapping $z \gtrsim 2$ LSS on $\sim$ Mpc scales, illustrating the challenge of using galaxy redshift surveys for this purpose, despite many hundreds of hours of large telescope time. In order to make galaxy maps with comparable resolution to our tomographic reconstructions, the galaxy number density needs to be increased dramatically, requiring 30 m class telescopes to obtain redshifts from faint ($R \gtrsim 26$) galaxies.

For these coeval galaxies, we determined their 3D positions within our map (overplotted on Figure 3) and evaluated the corresponding $\delta_F^{\rm rec}$. The $\delta_F^{\rm rec}$ sampled by these galaxies are shown in Figure 5(a), compared with the $\delta_F^{\rm rec}$ distribution from the full map; in Figure 5(c), we show the galaxy distribution as a function of the percentile of map ranked by flux (where larger flux
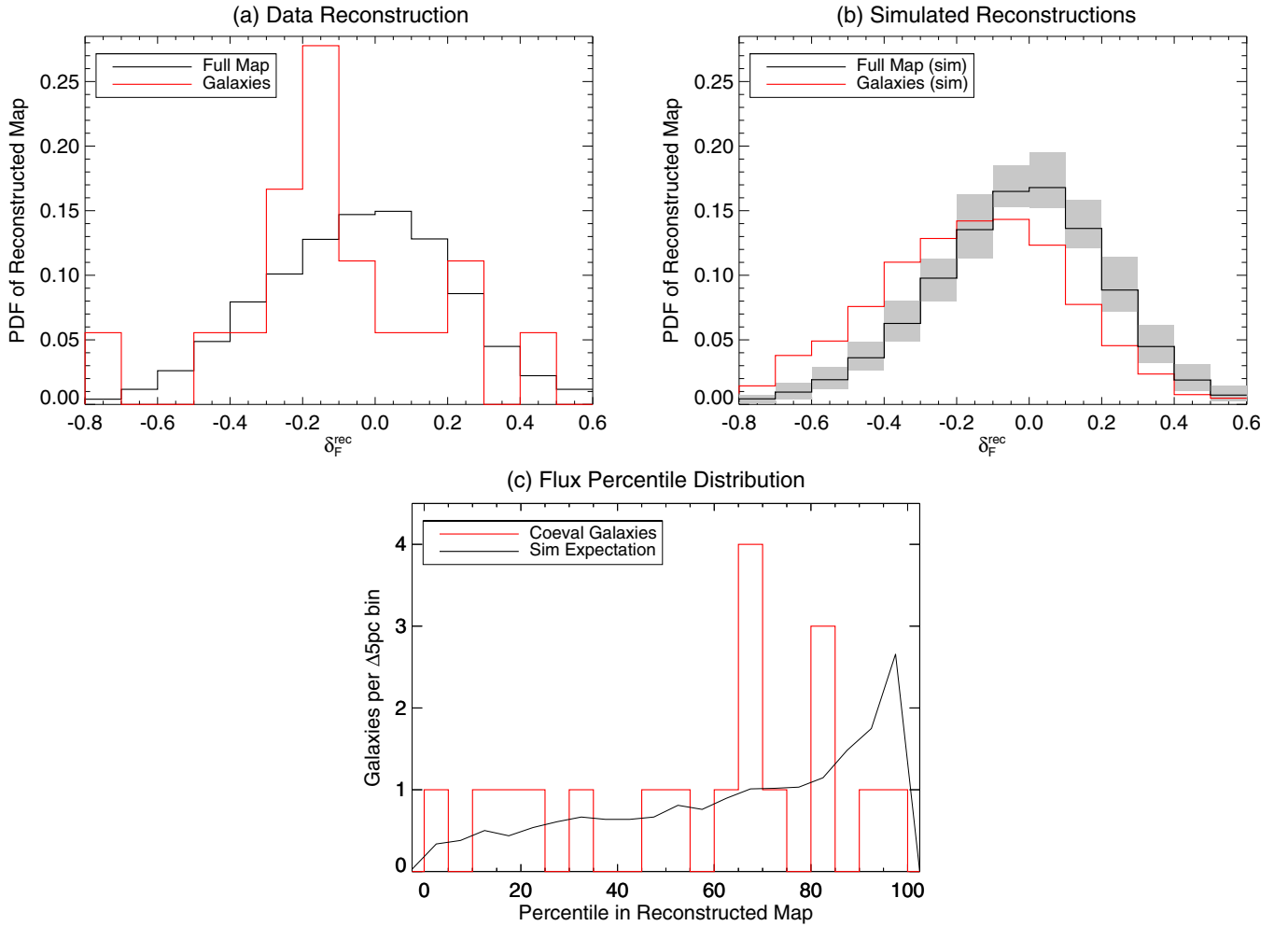
(a) Data Reconstruction

(b) Simulated Reconstructions

(c) Flux Percentile Distribution

Figure 5. (a) PDF of our tomographic map (black) compared with that sampled by 18 coeval galaxies within our map volume (red; both PDFs normalized to unit area). (b) Similar to panel (a), but evaluated over 24 mock reconstructions simulating the real map. The red curve shows the $\delta_F^{\rm rec}$ evaluated at 2506 simulated $R \leqslant 25.5$ galaxies within the mock reconstructions—the simulated galaxies clearly also preferentially live in low-$\delta_F^{\rm rec}$ regions. Shaded regions indicate the range of map PDFs from the 24 mock reconstructions, indicating the significant sample variance from the small volume. (c) Distribution of coeval galaxies as a function of the map flux percentile, such that $\delta_F^{\rm rec}$ decreases with the percentile, i.e., larger percentiles probe overdensities. The black curve indicates the predicted distribution from the simulated galaxies within our mock reconstructions.

(A color version of this figure is available in the online journal.)

percentiles represent overdensities). The galaxies preferentially occupy low-$\delta_F^{\rm rec}$ regions (i.e., overdensities) of the map.

However, at first glance, it seems troublesome that several galaxies are located in high-$\delta_F^{\rm rec}$ (underdense) regions. This could partly be due to errors in the galaxy spectroscopic redshifts; these are $\sigma_v \approx 300\,{\rm km\,s^{-1}}$ (Diener et al. 2013), i.e., $\sigma_\chi \approx 3.3\,h^{-1}$ Mpc along the line of sight at $z \approx 2.3$. This seems plausible for the galaxy at $[x_{\rm perp}, y_{\rm perp}, z] = [0.5\,h^{-1}\,{\rm Mpc}, 0.6\,h^{-1}\,{\rm Mpc}, 2.233]$ (top panel, Figure 3), which apparently occupies a void, but is in fact within $\pm 1\sigma$ of two overdensities on either side. Indeed, in Figure 3, most of the galaxies are within $\sim 1\sigma$ of significant overdensities. Another possible reason for this discrepancy could be different redshift–space distortions experienced by the galaxies and the forest; the latter has been constrained by Slosar et al. (2011) but has yet to be measured for $z \gtrsim 2$ galaxies.

Tomographic reconstruction errors (see Figure 4) could also decrease the correlation between the galaxies and 3D Lyα absorption, particularly in regions poorly sampled by sightlines. We investigate this using our simulations, from which we

extracted $R \leqslant 25.5$ galaxies through halo abundance matching (see L14 for details), introduced the expected line of sight redshift errors and then evaluated their positions within the mock tomographic reconstructions; this is illustrated by the mock galaxies in Figure 4. The distribution is shown in the red histogram in Figure 5(b), which shows a clear preference toward negative-$\delta_F^{\rm rec}$ (overdensities). This is also evident in Figure 5(c), which shows the distribution as a function of flux percentiles (normalized to $N = 18$ as in the real data). A two-sample Kolmogorov–Smirnov test between the percentile distribution of the real galaxies versus that from the simulations indicate a 22% probability of being drawn from the same distribution, which is reasonable considering the small data set. The long tail of galaxies in the underdensities is primarily due to a combination of galaxy redshift errors and reconstruction noise. The former could be mitigated in the near future by accurate systemic redshifts from near-IR spectroscopy, while to account for reconstruction noise we are developing methods to estimate the map covariance and hence characterize the uncertainties at any point within the maps.

5. CONCLUSION

We present the spectroscopic observations targeting, for the first time, high-redshift galaxies as background sources for Lyα forest analysis. This enabled us to create a tomographic map of the 3D absorption field with a spatial resolution of $\epsilon_{3D} \approx 3.5\,h^{-1}$ Mpc covering a comoving volume of $\approx (27\,h^{-1}\,\mathrm{Mpc})^3$ at $\langle z \rangle \approx 2.3$. Simulated tomographic reconstructions show that our sightline sampling, resolution, and S/N should yield a good recovery of the underlying absorption field. Supporting this conclusion, a sample of 18 coeval galaxies with known spectroscopic redshifts are found to preferentially occupy high-absorption regions (i.e., overdensities) in our map.

These results demonstrate the feasibility and promise of the full CLAMATO survey: $\sim$1000 SFGs at $z_{\mathrm{bg}} \sim$ 2–3 covering $\sim$1 deg^2 in the COSMOS field, which will enable a $\langle z \rangle \sim 2.3$ Lyα forest tomographic map with $\epsilon_{3D} \sim 3$–$4\,h^{-1}$ Mpc spatial resolution over a $(65\,h^{-1}\,\mathrm{Mpc})^2 \times 250\,h^{-1}$ Mpc $\sim (100\,h^{-1}\,\mathrm{Mpc})^3$ comoving volume. This will allow us to directly characterize the topology and morphology of $z > 2$ LSS for the first time—already we see tantalizing hints of structures extending across $\gtrsim 10\,h^{-1}$ Mpc in the high-redshift cosmic web. A large-volume LSS map will also enable a search for progenitors of massive $z \sim 0$ galaxy clusters—these protoclusters should manifest themselves at $z \gtrsim 2$ as overdensities of a few over $\sim 10\,h^{-1}$ Mpc (Chiang et al. 2013) scales. In a forthcoming paper, we will discuss methods to find protoclusters using Lyα forest tomography.

The proposed survey will create rich synergy with other COSMOS data sets. We would be able to study various high-redshift galaxy properties, e.g., morphology, color, and star formation rate, as a function of their environment within the cosmic web. Such studies will require the full $\sim (100\,h^{-1}\,\mathrm{Mpc})^3$ CLAMATO volume in order to sample enough objects to beat down the galaxies' redshift uncertainties and reconstruction errors, but promises unique insights into galaxy formation and evolution during the $z \sim 2$–3 epoch. Finally, CLAMATO will probe the small-scale clustering of the LSS, and will be highly complementary with wide-field surveys such as HETDEX (Hill et al. 2004) and DESI (Levi et al. 2013) to probe cosmological clustering over a broad range of spatial scales at $z \gtrsim 2$.

REFERENCES

Becker, G. D., Hewett, P. C., Worseck, G., & Prochaska, J. X. 2013, MNRAS, 430, 2067
Berry, M., Gawiser, E., Guaita, L., et al. 2012, ApJ, 749, 4
Bi, H., Ge, J., & Fang, L.-Z. 1995, ApJ, 452, 90
Brammer, G. B., van Dokkum, P. G., Franx, M., et al. 2012, ApJS, 200, 13
Busca, N. G., Delubac, T., Rich, J., et al. 2013, A&A, 552, A96
Capak, P., Aussel, H., Ajiki, M., et al. 2007, ApJS, 172, 99
Caucci, S., Colombi, S., Pichon, C., et al. 2008, MNRAS, 386, 211
Cen, R., Miralda-Escudé, J., Ostriker, J. P., & Rauch, M. 1994, ApJL, 437, L9
Chiang, Y.-K., Overzier, R., & Gebhardt, K. 2013, ApJ, 779, 127
Cisewski, J., Croft, R. A. C., Freeman, P. E., et al. 2014, MNRAS, 440, 2599
Croft, R. A. C., Weinberg, D. H., Bolte, M., et al. 2002, ApJ, 581, 20
Croft, R. A. C., Weinberg, D. H., Katz, N., & Hernquist, L. 1998, ApJ, 495, 44
Dawson, K. S., Schlegel, D. J., Ahn, C. P., et al. 2013, AJ, 145, 10
Delubac, T., Bautista, J. E., Busca, N. G., et al. 2014, arXiv:1404.1801
Diener, C., Lilly, S. J., Knobel, C., et al. 2013, ApJ, 765, 109
Hill, G. J., Gebhardt, K., Komatsu, E., & MacQueen, P. J. 2004, in AIP Conf. Proc. 743, The New Cosmology: Conference on Strings and Cosmology, ed. R. E. Allen, D. V. Nanopoulos, & C. N. Pope (Melville, NY: AIP), 224
Hui, L., Gnedin, N. Y., & Zhang, Y. 1997, ApJ, 486, 599
Ilbert, O., Capak, P., Salvato, M., et al. 2009, ApJ, 690, 1236
Koekemoer, A. M., Aussel, H., Calzetti, D., et al. 2007, ApJS, 172, 196
Lee, K.-G., Bailey, S., Bartsch, L. E., et al. 2013, AJ, 145, 69
Lee, K.-G., Hennawi, J. F., White, M., Croft, R. A. C., & Ozbek, M. 2014a, ApJ, 788, 49
Lee, K.-G., Hennawi, J. P., Spergel, D. N., et al. 2014b, arXiv:1405.1072
Lee, K.-G., Suzuki, N., & Spergel, D. N. 2012, AJ, 143, 51
Le Fevre, O., Tasca, L. A. M., Cassata, P., et al. 2014, A&A, submitted (arXiv:1403.3938)
Leitherer, C., Ortiz Otálvaro, P. A., Bresolin, F., et al. 2010, ApJS, 189, 309
Leitherer, C., Schaerer, D., Goldader, J. D., et al. 1999, ApJS, 123, 3
Levi, M., Bebek, C., Beers, T., et al. 2013, arXiv:1308.0847
Lilly, S. J., Le Fèvre, O., Renzini, A., et al. 2007, ApJS, 172, 70
McDonald, P., Seljak, U., Burles, S., et al. 2006, ApJS, 163, 80
Oke, J. B., Cohen, J. G., Carr, M., et al. 1995, PASP, 107, 375
Palanque-Delabrouille, N., Yèche, C., Borde, A., et al. 2013, A&A, 559, A85
Pichon, C., Vergely, J. L., Rollinde, E., Colombi, S., & Petitjean, P. 2001, MNRAS, 326, 597
Pieri, M. M., Mortonson, M. J., Frank, S., et al. 2014, MNRAS, 441, 1718
Press, W. H., Teukolsky, S. A., Vetterling, W. T., & Flannery, B. P. 1992, Numerical Recipes in FORTRAN. The Art of Scientific Computing (Cambridge: Cambridge Univ. Press)
Reddy, N. A., Steidel, C. C., Pettini, M., et al. 2008, ApJS, 175, 48
Salvato, M., Ilbert, O., Hasinger, G., et al. 2011, ApJ, 742, 61
Savaglio, S., Panagia, N., & Padovani, P. 2002, ApJ, 567, 702
Scoville, N., Aussel, H., Brusa, M., et al. 2007, ApJS, 172, 1
Shapley, A. E., Steidel, C. C., Pettini, M., & Adelberger, K. L. 2003, ApJ, 588, 65
Slosar, A., Font-Ribera, A., Pieri, M. M., et al. 2011, JCAP, 09, 001
Steidel, C. C., Shapley, A. E., Pettini, M., et al. 2004, ApJ, 604, 534
White, M., Pope, A., Carlson, J., et al. 2010, ApJ, 713, 383
Wiener, N. 1942, The Interpolation, Extrapolation and Smoothing of Stationary Time Series (Cambridge, MA: MIT Press)
Zaroubi, S., Hoffman, Y., Fisher, K. B., & Lahav, O. 1995, ApJ, 449, 446